Experimental and numerical study of fracture mechanisms of UO_2 nuclear fuel

J-M Gatt[a], J. Sercombe[b], I. Aubrun[c] and J-C Ménard[d]

CEA, DEN, DEC Cadarache

13108 St Paul Lez Durance, France

[a]jean-marie.gatt@cea.fr, [b]jerome.sercombe@cea.fr, [c]isabelle.aubrun@cea.fr,

[d]jean-claude.menard@cea.fr

Keywords: fracture, bending tests, indentation tests, nuclear fuel

Abstract: In this paper we study the brittle behavior of UO_2 nuclear fuel. First, we present the interpretation of bending tests with three different approaches to evaluate rupture parameters (critical stress and toughness). Second, we present Vickers indentation tests on fresh UO_2 fuel. The comparison between bending and indentation tests on fresh fuel allows us to evaluate the constant parameters relative to indentation tests. Vickers indentation is then used to evaluate rupture parameters of irradiated fuels. At the end, we present some applications to fuel rod modeling taking into account the different rupture mechanisms.

Introduction

This paper deals with the rupture of UO_2 fuel in a nuclear reactor. At low temperature (up to 900 °C), this ceramic is brittle. We show that the fracture network has an important impact on the loading of clad due to pellet expansion (thermal expansion and swelling). The goal of this article is to present a methodology to study this problem. The measurement of rupture parameters (ultimate stress and toughness) is therefore important to have a good simulation of pellet cladding interaction in different operating conditions. For that, we must develop a methodology to evaluate rupture parameters on fresh fuel and irradiated fuel. This paper is divided into three parts. The first part shows how we measure the rupture parameter using bending tests. An interpretation of these tests using modeling is necessary to identify the real different parameters of the models (cohesive zone model and DDIF2 [1]). In the second part of this paper we present measurements by Vickers indentation. The interest in these tests is that it can be used on irradiated fuel. The last part of the article, describes the modeling used to simulate a fuel rod taking into account the different rupture mechanisms.

Bending tests on fresh fuel

We have performed bending tests on samples with and without notch. The first tests are used to measure rupture stress and the second to measure toughness. Four kinds of samples are tested: Large samples (28x4x4 mm^3) and small samples (10x1.5x1.5 mm^3) of UO_2 with large and small grain size. The fuels are porous and the microstructures of samples are very different from each other. We define the rupture stress of a sample submitted to bending test by:

$$\sigma_R = \frac{3L}{2be^2} F_R \qquad (1)$$

L, b, e are respectively the length, the width and the thickness of the sample. F_R is the force measured at the time of rupture. The rupture of a sample is controlled by two parameters:

critical stress and resilience or toughness. Resilience G_c and toughness K_c are linked by the following equation (in plane stress conditions):

$$G_c = \frac{K_c^2}{E} \tag{2}$$

with E the Young's modulus.

To interpret the bending tests and to find the relationship between rupture stress, critical stress and toughness, we need numerical simulation. We propose three approaches described below: two finite elements approaches (cohesive zone model and using the DDIF2 model [1]) and an analytical approach.

Cohesive zone model. According to Fig. 1, we have the following equations:

$$\begin{cases} K_n = \dfrac{\sigma_c}{\delta} \\ G_c = \dfrac{1}{2}\sigma_c(\delta_c - \delta) \\ K_f = \dfrac{\sigma_c}{\delta_c - \delta} \end{cases} \tag{3}$$

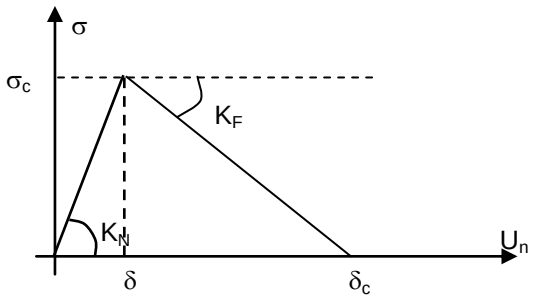

Fig. 1: cohesive zone model

So we obtain the following behavior law for cohesive zone model:

$$\sigma_n = \begin{cases} K_n u_n & \text{if} \quad u_n < \delta \\ \left(\dfrac{\delta - u_n}{\delta_c - \delta} + 1\right)\sigma_c & \text{if} \quad \delta \le u_n \le \delta_c \\ 0 & \text{if} \quad u_n \ge \delta_c \end{cases} \tag{4}$$

with σ_c the critical stress. Note that σ_c is different from σ_R.

The following condition has to be verified for the consistency of the model:

$$K_n > \frac{\sigma_c^2}{2G_c} \tag{5}$$

Using the mesh shown **Fig. 2**, a resilience value and a critical stress allowing to find again the experimental rupture stress, Fig.3 gives the results of the simulation of bending test.

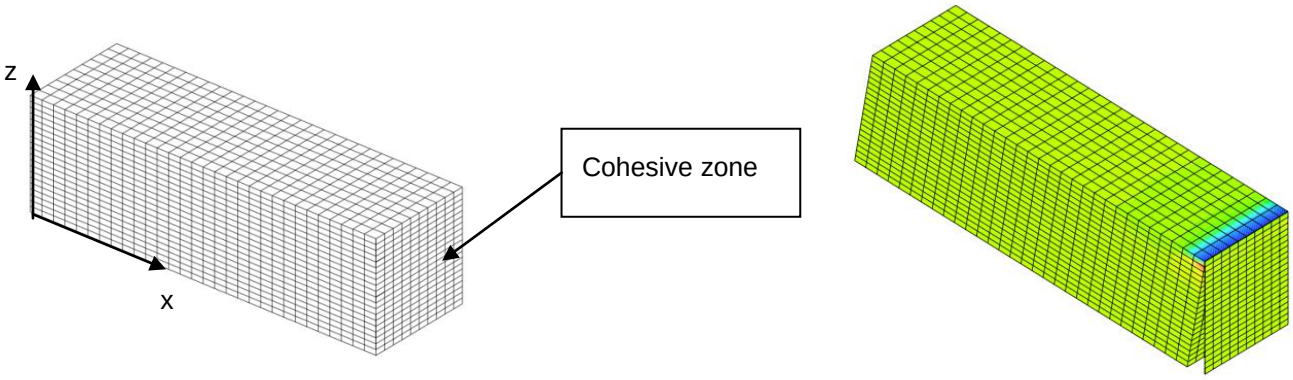

Fig. 2 : meshing of sample and sample at the end of simulation

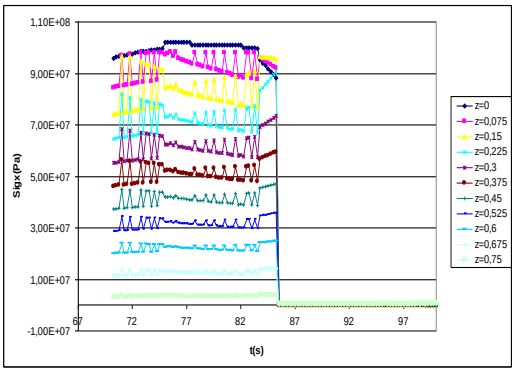

Fig.3a: stress (σ_x) evolution versus thickness (z) and time

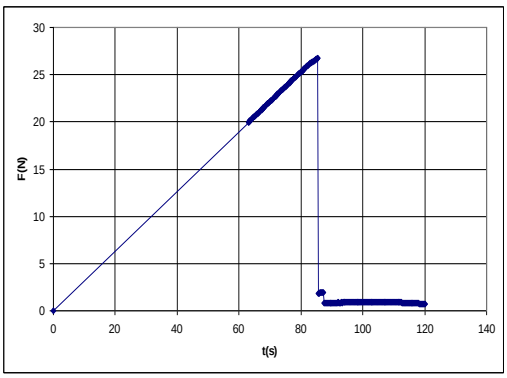

Fig.3b : force evolution versus time

From Fig.3a, we can estimate the crack initiation length to be between 75 µm and 150 µm.

DDIF2 model [1]. According to Fig. 4, we have the following equations:

$$E_{fisi} = \frac{1}{2}.\frac{\sigma_{c,i}^2}{G_{ci}}.L_i \qquad (6)$$

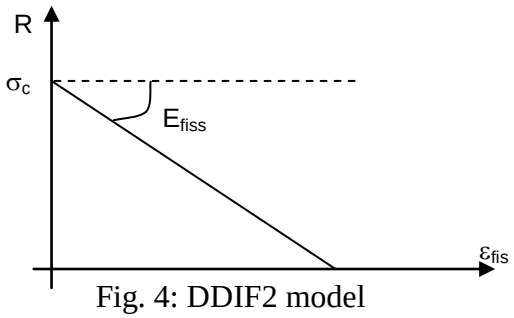

Fig. 4: DDIF2 model

The indix i is linked to the direction of crack (x, y, z) and L_i is the finite element length which is perpendicular to the crack plane. The link between crack strain rate $\dot{\varepsilon}_{fis}$ and stress is deduced from the consistence condition:

$$d\vec{f}_{fis}.\vec{e}_i = \frac{\partial\left(\vec{f}_{fis}.\vec{e}_i\right)}{\partial\sigma} : d\sigma + \frac{\partial\left(\vec{f}_{fis}.\vec{e}_i\right)}{\partial R} : dR = n_i : \left[d\sigma - \frac{\partial R}{\partial \varepsilon_{fis}} : d\varepsilon_{fis} \right] = 0 \qquad (7)$$

R is the resistance tensor ($R_{ii\,max} = \sigma_{cii}$).
Using symmetries of resistance tensor R, we show that the crack strain rate tensor in each direction reads:

$$n_i : \dot{\varepsilon}_{fis} = \frac{n_i : \dot{\sigma}}{n_i : \frac{\partial R}{\partial \varepsilon_{fis}} : n_i} \tag{8}$$

Finally, we use mechanical behavior law to link stress rate tensor and strain rate tensor:

$$\dot{\sigma} = C : \left(\dot{\varepsilon} - \dot{\varepsilon}_{fis}\right) \tag{9}$$

Analysis of bending tests. Using the DDIF2 model we have simulated bending tests. In Fig. 5, we can see the results of a simulation. The crack propagation is represented in the center of the sample.

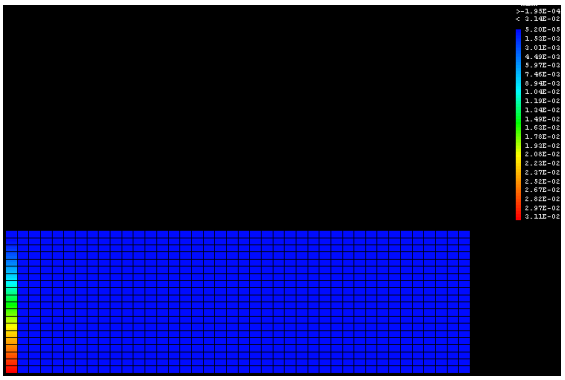

Fig. 5: Result of simulation with DDIF2 model

We have also simulated three points bending tests on notched sample.

Fig. 6 shows the mesh used.

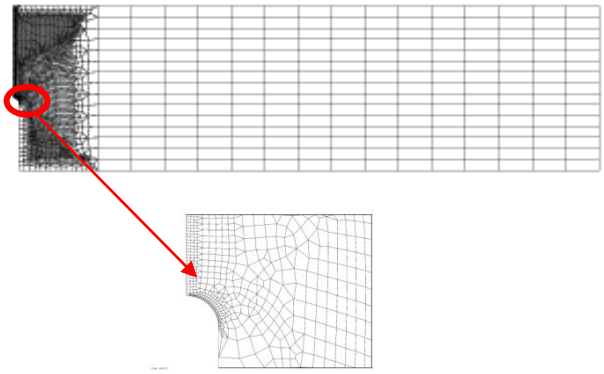

Fig. 6 : mesh of notched sample

We obtain the results shown Fig.7.

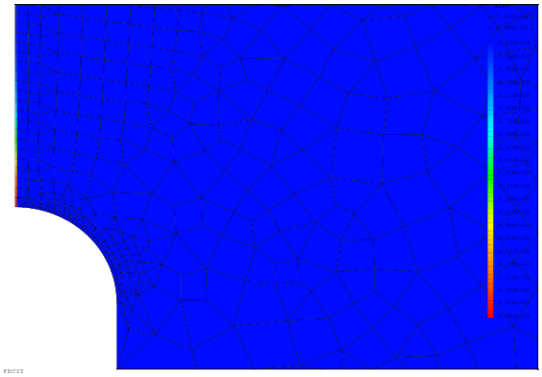

Fig.7a: simulation results.

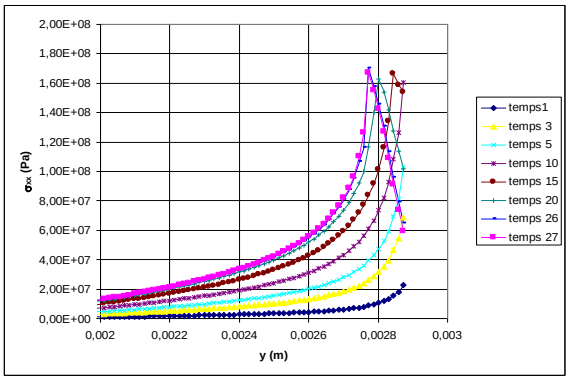

Fig.7b: Stress evolution along the ligament.

From Fig.7b, we can evaluate the crack critical length at 600 µm. The test interpretations on samples with and without notch show that the crack initiation length is great enough in comparison to grain size and default sizes to conclude that measurements of toughness and critical stress are macroscopic. These are not local measurements.

Analytical model: Now, we propose to use an analytical approach to interpret the bending tests. This approach, introduced by D. Leguillon [2], allows us to study the rupture of bending sample using an energy and critical stress. These two criteria read:

Stress criteria:

$$k(x)\sigma_{max} \geq \sigma_c \qquad \textbf{(10)}$$

with : $\sigma_{max} = \frac{3FL}{2be^2}$, $x = \frac{d}{e}$ and : $k(x) = 1 - \frac{2d}{e} = 1 - 2x$, « d » being the distance between the central point the more loaded in traction (d=0 or x=0) and situated on the symmetric axis of the sample. (d=e/2 ou x=1/2 is a neutral axe). These notations are specified Fig. 8.

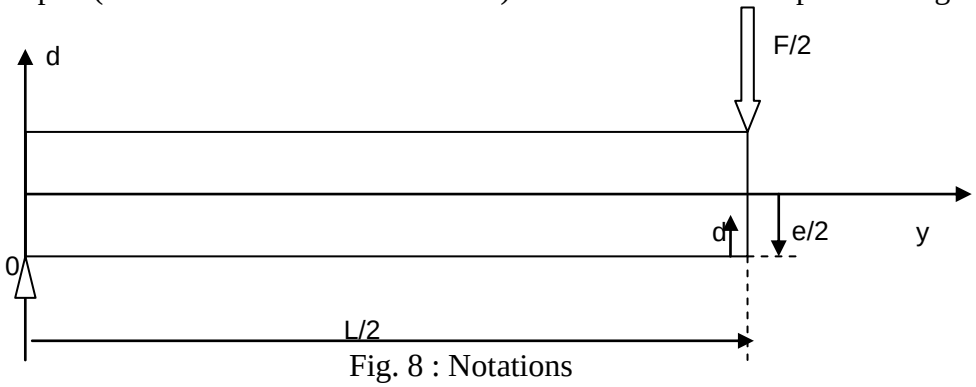

Fig. 8 : Notations

Energy criteria:

$$A(x)\sqrt{e}\sigma_{max} \geq K_c \qquad (11)$$

Using [3] we have for a bending sample:

$$K_c = Y\frac{F_R}{b\sqrt{e}} \quad \text{with} \quad F_R = \frac{2be^2}{3L}\sigma_R$$

$$Y = \frac{3\frac{L}{e}\sqrt{x}}{2(1+2x)(1-x)^{1,5}}\left[1{,}99 - x(1-x)(2{,}15 - 3{,}93x + 2{,}7x^2)\right] \quad \text{and} \quad \left(x = \frac{a}{e}\right) \tag{12}$$

To define the A function we can use equation (12). In this case we have:

$$A(x) = \frac{\sqrt{x}P(x)}{(1+2x)(1-x)^{3/2}} \tag{13}$$

With: $P(x) = 1{,}99 - x(1-x)(2{,}15 - 3{,}93x + 2{,}7x^2)$

The function A is plotted in Fig. 9. We have for $x \in [0,1]$ the following properties:

- A(0)=0
- A is continuous and strictly increasing
- A tends towards infinity when x tend towards 1

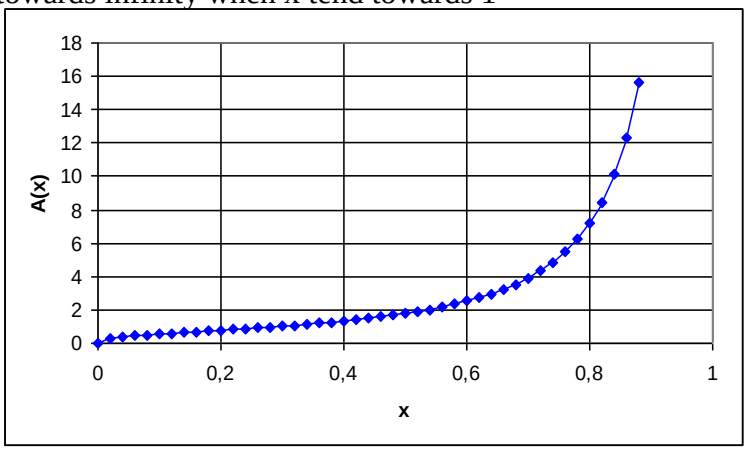

Fig. 9 : A function

The two conditions (10) and (11) are verified if:

$$\begin{cases} A(\hat{x})\sqrt{e} = k(\hat{x})\dfrac{K_c}{\sigma_c} \\ k(\hat{x})\sigma_R = \sigma_c \end{cases} \tag{14}$$

$\hat{d} = \hat{x}e$ is the crack initiation length. The last equation of system (14) gives the link between the rupture stress σ_R and critical stress σ_c. The crack initiation length is obtained thanks to the following equation.

$$A(\hat{x}) = \frac{K_c}{\sigma_R\sqrt{e}} = \sqrt{\frac{\beta E G_c}{e\sigma_R^2}} \tag{15}$$

According to the second equation of system (14) and equation (10) we have:

$$\frac{\sigma_c}{\sigma_R} = 1 - 2\hat{x} \tag{16}$$

Using equations (15) and (16) we can plot the intrinsic curve presented in Fig. 10.

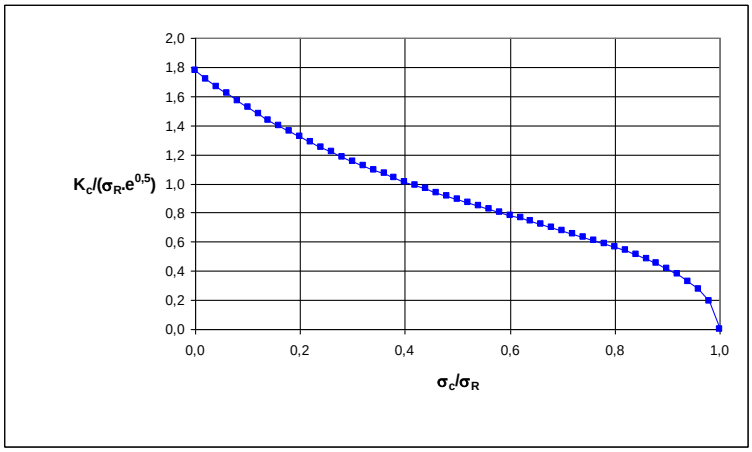

Fig. 10 : Curve allowing evaluating critical stress versus rupture stress and toughness

With this approach we can evaluate the crack initiation length using equation (15) for a bending test. This crack initiation length is given Fig. 11 for small and large samples. For small samples (thickness 1.5 mm), we obtain a crack initiation length between 40 µm and 110 µm. This length is great enough to consider that the critical stress is a macroscopic quantity taking into account the flaws (porosity) in the material. The crack initiation length should be significantly lower to measure the local value.

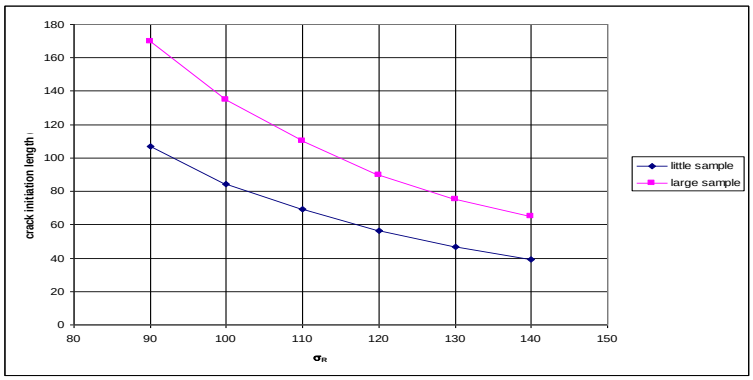

Fig. 11 : crack initiation length for large and small samples versus rupture stress

Comparison of different approaches: The crack initiation length evaluated by simulation on samples without a notch (between 75 and 150 µm) is in good agreement with that observed by the analytical approach (between 65 and 170 µm). Finally, Fig. 12 shows a comparison of the three approaches allowing evaluating the link between rupture and critical stress. We can observe a very good agreement between these three approaches.

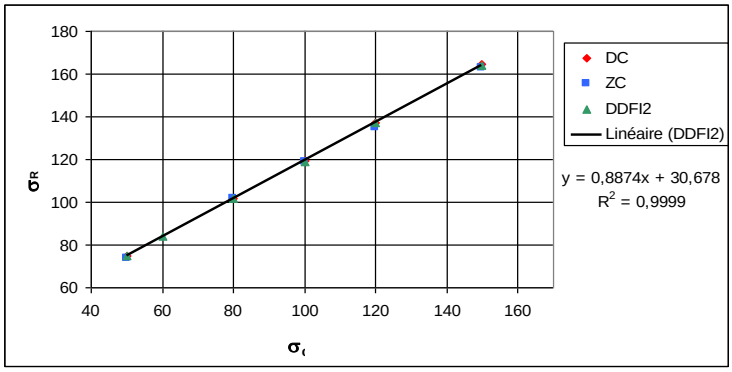

Fig. 12 : Comparison of three modeling approaches: cohesive zone, DDIF2 model and analytical

Analysis of bending tests with and without notched samples: Using equation (1), for each test we can evaluate the rupture stress. In the other hand, we can evaluate toughness using equations (12) and bending tests on notched samples. With these data and equations (15)(16) we evaluate the critical stress which must be used in the models. In Fig. 14, we show some results obtained from bending tests.

Vickers indentation tests analysis

Toughness: The indentation tests consist in punching a material with an indenter by imposing a normal force. After unloading, if the loading is high enough we observe four cracks as shown in Fig. 13. Two kinds of cracks can appear: Palmqvist crack (P) and median cracks (M) as shown in Fig. 13.

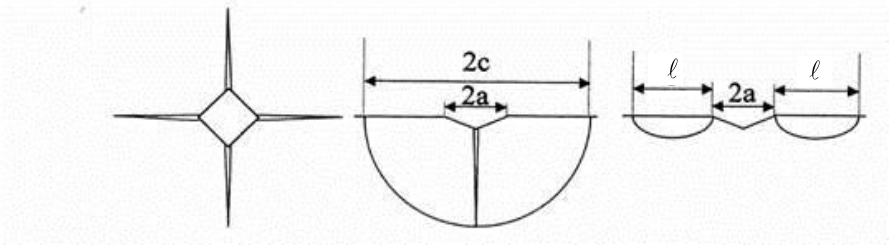

Fig. 13 : a) Diagram of indentation surface, b) Median type crack (M) c) Palmqvist type crack (P)

Usually, it is difficult to know the mechanism activated. So we propose to use arbitrary simple criteria: if c>2a we consider the mechanism M. This criterion allows us to obtain a good interpretation or our measurements. For M type cracks we use the following equation [4] [5]:

$$K_c = \kappa_M \sqrt{\frac{E}{H}} \frac{P}{c^{3/2}} \qquad (17)$$

E is the Young modulus, H the hardness, P the loading and κ_M a constant

In the same way, K. Niihara [7] proposes the following equation for P type cracks:

$$K_c = \kappa_P \left(\frac{E}{H}\right)^{2/5} \frac{P}{a\ell^{1/2}} \qquad (18)$$

κ_P is a constant for this mechanism.

Critical stress: To obtain all rupture parameters used in modeling, an evaluation of critical stress is essential, especially to study irradiated fuels. To reach this goal we have to consider a fictive bending test on a sample after indentation. During the bending test, after a stable propagation of damage, the crack due to indentation becomes instable from a limit loading. To interpret this test we have to consider two stress intensity factors: the first proportional to $P/c^{3/2}$ (it decreases when the crack increases) due to indentation and the second proportional to $\sigma c^{1/2}$ (it increases when the crack increases) due to bending test. The global stress intensity factor reads [6]:

$$K = \kappa_M \sqrt{\frac{E}{H}} \frac{P}{c^{3/2}} + \zeta_M \sigma \sqrt{c} \tag{19}$$

The crack is instable if:

$$\frac{\partial K}{\partial c}(c_L) = 0 \quad \text{and} \quad K_c = K(c_L) \tag{20}$$

Finally we find:

$$\begin{cases} K_c = 4\kappa_M \sqrt{\frac{E}{H}} \frac{P}{c_L^{3/2}} \\ K_c = 4\left(\frac{\kappa_M \zeta_M^3}{27}\right)^{1/4} \left(\frac{E}{H}\right)^{1/8} \left(\sigma_c^3 P\right)^{1/4} \\ K_c = \frac{4\zeta_M}{3} \sigma_c \sqrt{c_L} \end{cases} \tag{21}$$

Using (17) and (21) we find the following relation for crack type M:

$$\sigma_c = \frac{3}{4^{4/3}} \frac{\kappa_M}{\zeta_M} \left(\frac{E}{H}\right)^{1/2} \frac{P}{c^2} \tag{22}$$

With the same approach for cracks of type P, we find:

$$\sigma_c = \frac{1}{4} \frac{\kappa_P}{\zeta_P} \left(\frac{E}{H}\right)^{2/5} \frac{P}{a\ell} \tag{23}$$

Equations (17)(18) for toughness and (22)(23) for critical stress allow us to evaluate rupture parameters. All these parameters can be considered as macroscopic, because the length of the cracks (20 μm) is long enough in comparison to the grain and porosity sizes and the small enough in comparison to the thickness of bending sample used in this work.

Identification: The indentation tests were carried out on the same material as that used for bending tests. First, we identify the constants associated to toughness. For that, we use the results obtained with bending tests on notched samples. We find:

$$\kappa_M = 0.0432 \text{ and } \kappa_P = 0.00445$$

Second, we identify the constants associated to critical stress. We find:

$$\zeta_M = 2.3404 \text{ and } \zeta_P = 1.24114$$

Fig. 12 shows the comparison of results obtained by bending tests and Vickers indentation tests. We can conclude that:

- We have an important dispersion of results in indentation tests on UO_2

- The P and M mechanisms are activated for UO_2 small grain size and M for UO_2 large grain size
- The order of magnitude of different parameters and their relative evolution are in good agreement.

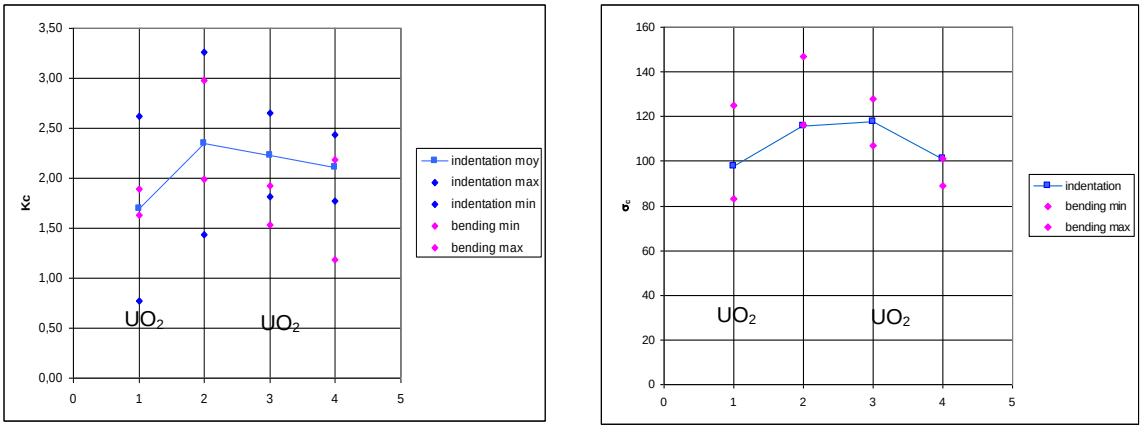

Fig. 14 : Comparison between indentation and bending tests (**1**: small UO_2 sample, **2**: small UO_2 sample with large grain size, **3**: large UO_2 sample and **4**: large UO_2 sample with large grain size)

Irradiation effects: We have used equations (17)(18) for toughness and (22)(23) for critical stress to study the irradiation effect. In figures (Fig. 15 and Fig. 16) we show a comparison between rupture parameters for fresh and irradiated fuels.

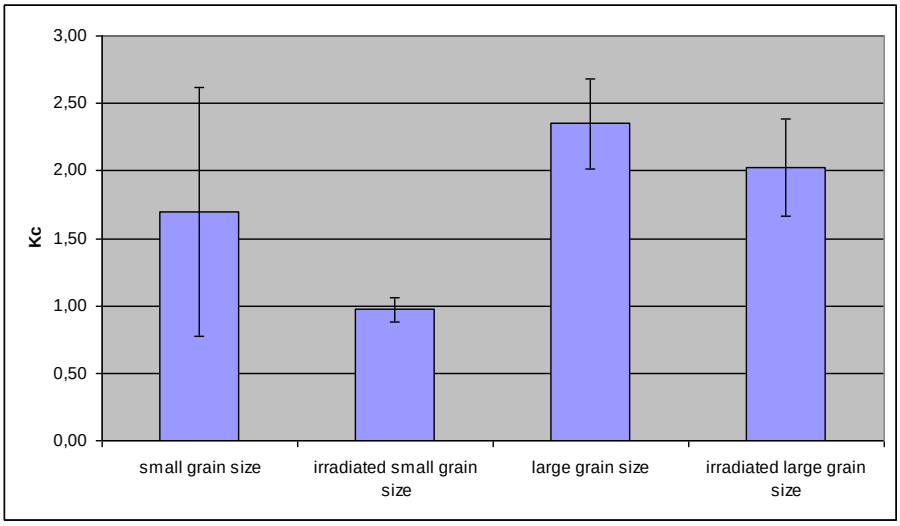

Fig. 15 : Comparison of toughness between fresh fuel and irradiated fuels

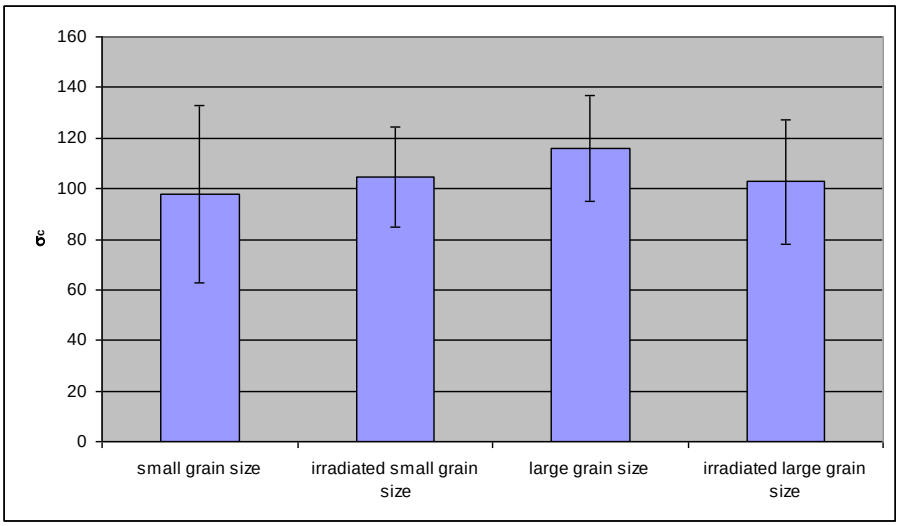

Fig. 16 : Comparison of critical stress between fresh fuel and irradiated fuels

We see that the evolution of critical stress is small compared to toughness evolution.

Application

These parameters are then used in the multi-dimensional fuel code ALCYONE [8][9] to model UO_2 cracking during reactor normal and off-normal loading conditions. In brief, ALCYONE describes the thermal-mechanical behaviour of cylindrical fuel pellets (typical dimensions are 8 mm diameter and 13 mm height) stacked in a Zircaloy cladding (external diameter 9 mm). During in-reactor irradiation, pellet thermal expansion and cladding creep due to the external coolant pressure (150 bars in a Pressurized Water Reactor) leads to the closing of the initial pellet-clad gap (80 microns). In case of power transients, stresses in the cladding due to this mechanical interaction can increase considerably. The release at the same time of corrosive products from the irradiated fuel pellets can lead to the failure of the cladding by a Stress Corrosion Cracking (SCC) mechanism. Fuel radial and axial cracking can relax considerably the stresses at the pellet clad interface and must therefore be accounted for when modelling in-reactor fuel behaviour. Fig. 17 gives an illustration of the fuel pellet radial cracking at the end of a 2D(r,θ) plane strain simulation of a power transient using the DDIF2 model. The elements in blue in the pellet are those where the dissipated energy exceeds the fracture energy. Due to the high thermal gradient that exists between the pellet center (≈ 2000°C) and its periphery (≈ 600°C), high circumferential and axial tensile stresses appear at the pellet periphery. When the tensile strength is exceeded, radial cracks are initiated and propagate more or less rapidly inside the pellet depending on the resilience. The cract network is consistent with experimental observations of fuel pellets after power transients, see Fig. 17.

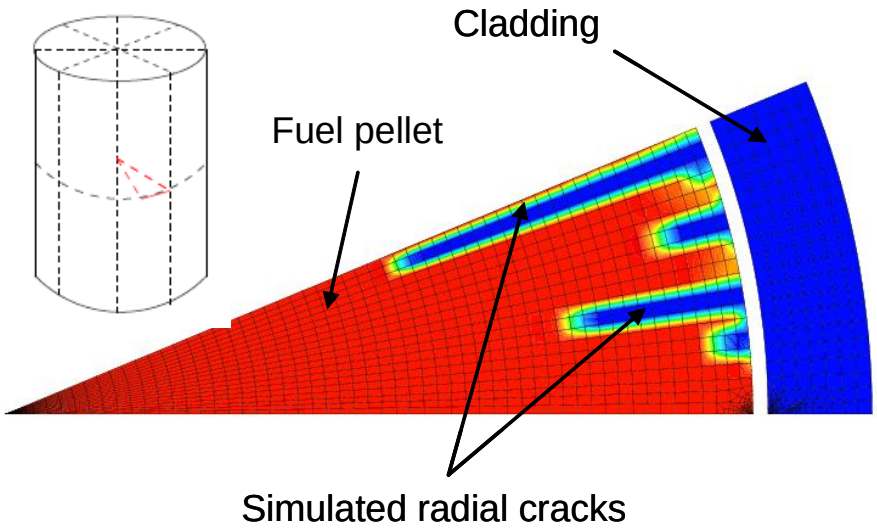

Fig. 17: ALCYONE 2D(r,θ) simulation showing the propagation of radial cracks in the fuel pellet at the end of the power transient.

Summary

We have presented a methodology based on Vickers indentation tests to evaluate rupture parameters of irradiated fuel. This approach is based on the study of rupture parameters of fresh fuel using the bending tests and the indentation tests. First, we have presented the link between the simulation and the bending test to define the scale of measurements and the relation between the rupture force measured during bending test and rupture parameters introduced in the models. Second, after a validation of numerical simulation thanks to an analytical approach, we have presented an interpretation of Vickers tests on irradiated fuel. We have shown that critical stress is not a parameter that allows differentiating the different irradiated fuels (UO_2 small and large grain sizes). Otherwise, we have shown that toughness is the main parameter. Finally, we have presented an application to a problem of pellet cladding interaction taking into account the DDIF2 model.

Knowledge

The authors thank EDF and AREVA NP for their technical and financial support for fuel mechanical behavior studies.

References

[1] B. Michel, J. Sercombe, D. Thouvenin, R. Chatelet, 3D Fuel cracking modeling in pellet cladding mechanical interaction, Eng. Fract. Mech. 75, pp3581-3598, 2008

[2] D. Leguillon, Strenght or toughness. A criterion for crack onset at a notch, Eur. J. Mech/ A/Solids, 21, pp. 61-72, 2002

[3] T.L. Anderson, Fracture Mechanics. Fundamentals and applications, Library of congress, ISBN 0-8493-4277-5, 1991

[4] B.R. Lawn, A.G. Evan, A model for crack initiation in elastic/plastic indentation fields, J. Mat. Sci., 12, pp2195-2199, 1977.

[5] D. Chicot, A. Pertuz, F. Roudet, M.H. Staia, J. Lesage, New developments for fracture toughness determination by Vickers indentation, Mter. Sci. Tech., 20, pp 877-884, 2004

[6] B.R. Law, D.B. Marshall, J., Residual stress effects in failure from flaws, J. of the American Cer. Soc., Vol 62, N°1-2, 1979

[7] K. Niihara, A fracture mechanics analysis of indentation-induced Palmqvist crack in ceramics, J. of Mat. Sc. Let. 2, pp221-223, 1983

[8] B. Michel, J. Sercombe, G. Thouvenin, A new phenomenological criterion for Pellet Cladding Interaction rupture, Nuclear Eng. And Design, 238, pp1612-1628, 2008.

[9] J. Sercombe, I. Aubrun, C. Nonon, Power ramped cladding stresses and strains in 3D simulations with burnup-dependent pellet–clad friction, Nuclear Eng. And Design, 242, pp164-181, 2012.